Friction stir welding of EH46 steel grade at dwell stage: Microstructure evolution

AL-MOUSSAWI, M., SMITH, Alan <http://orcid.org/0000-0001-7868-8501> and FARAJI, M.

Friction Stir Welding of EH46 steel grade at Dwell Stage: Microstructure Evolution

*[1] M. Al-moussawi, *[2] A.J Smith, [3]M. Faraji
*[1,2]Sheffield Hallam University/MERI/UK, [3]Coventry University
*[1]b1045691@my.shu.ac.uk +447462954845
*[2] engajs@exchange.shu.ac.uk

Abstract

This work aims to understand the effect of changes in Friction Stir Welding (FSW) process parameters on the resulting microstructure specifically the effect of the plunge depth and tool rotational speed, during the "dwell" period on the resulting microstructure. A series of (FSW) of 14.8mm thick EH46 steel plate using a hybrid Poly Crystalline Boron Nitride (PCBN) FSW tool with spindle speeds of 120 and 200 revolutions per minute have been produced with increasing plunge depths from 0.1mm to 0.7mm. Thermo-couples embedded around the top surface of each plunge case were used to measure the peak temperature during the process. The plunge depths were measured using the infinite focus microscopy and the microstructure of all the heat affected regions was investigated extensively by scanning electron microscopy. It was found that phase transformation is sensitive to the variation on plunge depth. Small increase in plunge depth caused a significant change in the microstructure. Increasing tool rotational speed was also found to cause a significant difference in the microstructure.

Keywords: EH46 steel, Friction Stir welding, Plunge Depth, microstructure.

1. Introduction

Friction Stir Welding (FSW) was invented by The Welding Institute (TWI) in 1991 [1], FSW is a solid state welding process in which a rotating tool, is plunged into the gap between the materials to be joined and held until the material starts to yield, the tool is then moved linearly down the welding line until the join is completed. Finally the tool is raised from the joint; leaving a deep indentation in the workpiece. The process was initially limited to light alloys such as Al and Mg because FSW of higher melting point materials such as steel required the use of a very expensive welding tool (usually hybrid Poly Crystalline Boron Nitride-Tungsten Rhenium PCBN-WRe or Tungsten Carbide-Cobalt WC-Co) which represent 99% off the total machine direct cost [1]. The process of the FSW especially in steel alloys is also complicated by the fact that the process produces high strain and high strain rates which create significant heat and promotes microstructural phase transformations. The initial plunge and dwell stages which are similar to friction stir spot welding (FSSW) represent the most important stages in which the material gains the required heat to yield before the tool traverses down the welding line at a steady state. Previous work on microstructure evolution during the dwell stage and especially for steel is limited. Feng et al. 2005 [2] have investigated the microstructure of the base metal, Heat Affected Zone (HAZ) and Thermo-Mechanical Affected Zone (TMAZ), and hardness in FSSW of two types of steel M-190 and DP600 by using PCBN FSW tool. They found that the material in the HAZ had experienced a phase transformation with peak temperature between the A_1 and A_3 temperature. The microstructure in the thermo-mechanical affected zone (TMAZ) was also

examined and it was suggested that this region also experienced a peak temperature above the A_3 line in the Fe-C phase diagram. Their work did not include a variation in welding parameters as the weld was produced at a pre-determined depth with a fixed tool rotational speed. Lomholt et al. 2012 [3] investigated the microstructure and feasibility of FSSW of transformed induced plasticity (TRIP) steel, the microstructure was subdivided into four zones; two TMAZ and two HAZ's. Ultra-fine grained ferrite was found in both of the TMAZ regions and interpreted as a result of severe deformation at an elevated temperature.

Mazzaferro et al. 2015 [4] applied FSSW on TRIP steel to investigate the microstructure and mechanical properties with the influence of dwell time and tool rotational speed. It was found that allotriomorphic ferrite in the TMAZ increased with increasing dwell time and tool rotational speed and to obtain a high strength lap-shear, a lower rotational speed and higher dwell time is required. Hovanski et al. 2007 [5] studied the effects of FSSW parameters such as tool rotational speed and cycle time on properties and phase transformation of hot-stamped boron steel. They found that plunge depth is the most important parameter which can affect the strength of the TMAZ. Miles et al. 2012 [6] investigated the FSSW of high strength steel at high rotational speed and showed that increasing tool rotational speed had caused an increase in the resulting joint impact strength.

In the current work the effects of welding parameters such as tool rotational speed and plunge depth on the resulting microstructure were investigated. A hybrid PCBN tool was employed to produce seven plunge holes in 14.8mm thick plate of EH46 steel grade as shown in Figure 1. Thermocouples embedded inside 1mm blinds holes were used to record the peak temperatures. SEM test was employed to examine the microstructure in the different thermo-mechanically affected zones. The thermo-mechanical effect of each part of the tool including shoulder, probe side and probe end on the microstructure were also investigated. The effect of axial (plunge force) was not taken into consideration as it could have added more complexity to the process analysis.

2. Experimental Procedure

2.1 FSW Tool and Workpiece Material. The FSW tool used to carry out the welding is a hybrid PCBN-WRe with a shoulder diameter 38mm and probe length 12mm. The parent material used in the welding trials was an EH46 steel grade plate of 14.8mm thickness; the chemical composition is shown in Table 1.

Table 1: Chemical composition of EH46 Steel Grade

C	Si	Mn	P	S	Al	N	Nb	V	Ti
0.20	0.55	1.7	0.03	0.03	0.015	0.02	0.03	0.1	0.02

The position of the individual weld plunges and the six thermocouples was carefully mapped to increase the accuracy of temperature measurements and to enable a correlation between these temperatures and the resulting microstructure. Seven weld plunge trials were carried out at TWI Yorkshire using a PowerStir FSW machine. The machine was specifically designed for welding thick section and high melting point materials. The machine is a moving gantry

2

design and has been built to withstand the high forces with minimal structural deflection. The weld samples of plunge trail welds are numbered W1 to W7 (Table 2).

2.2 Plunge Feed-rate.

The PowerStir FSW machine had the ability to record welding parameters such as force, torque, rotational speed, feed rate and plunge/dwell time. The plunge depth feed-rate decreases as the tool is depressed into the surface of the material. For W1 and W2 the plunge depth feed-rate started at 10mm/min, decelerated to 5mm/min and finally 3mm/min before reaching the maximum plunge depth. For weld plunge trials W3 to W7 the plunge depth feed-rate decreased from a maximum of 7mm/min to 3mm/min before reaching the maximum plunge depth. The plunge depth recorded by the machine has not been used in this work because of concern over a possible error due to machine deflections during processing. Therefore, resulting plunge depths following each of the trials have been measured using the Infinite Focus Microscope (IFM). The Infinite Focus Microscope (IFM) is a rapid non-contact optical 3D measurement device, which combines the low depth of field of an optical microscope with vertical scanning, traversing across the surface of the sample, to provide high resolution and high depth of field topographical images with a large field of view. The scanned area of interest can be transferred into a 3-D image, and then the surface area can be calculated accurately.
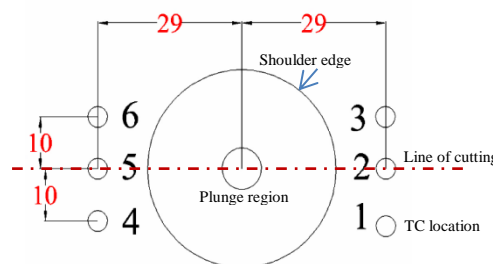
2.3 Tool Rotational Speeds.

Rotational speeds in the dwell period were 200RPM for W1 and W2 and 120RPM for all other cases.

Figure 1: EH46 steel plate showing the position of the seven plunge trials.

Thermocouples were inserted in blind holes (1mm depth) inside the plates and fixed firmly at 29mm away from the tool center of the EH46 plunge trials as shown in Figure 2.

Fig. 2: Thermo-Couples (TC) locations around each plunge trial.

2.4 Sample preparation for microscopic examination using the SEM and Infinite Focus Microscope (IFM).

The IFM has been used to accurately measure the depth of each plunge cavity before cutting the samples into two halves. Each of the plunge cavities were cut in half in the direction perpendicular to the thermocouple location as shown in Figure 2 (line of cutting). Samples were then polished to 1 micron finish and etched in 2% Nital to reveal the microstructure.

2.5 SEM: Scanning electron microscopy examinations were carried out on the polished and etched samples for each of the plunge trials so that the various TMAZ and HAZ could be identified, characterised and/or measured. The main aim for this microstructural assessment is to generate information regarding the phases that are likely to be present in the TMAZ and HAZ. The grains sizes in the microstructure were measured using the mean linear intercept method.

3. Results and Discussion.

3.1 Macrographs and measurements for temperatures and plunge depth:

Table 2 shows the FSW conditions and plunge depth measurements for each trial of the weld (W1 to W7).

**Table 2: The welding conditions and the measurements of plunge depth.**

Weld Trial No.	Tool rotational speed ω (RPM) at maximum plunge depth	Max. Axial (Plunge) force (F_z) KN	Max. Traverse force (F_x) KN	Max. Torque (M) N.m	Plunge Depth (Z) mm (IFM)	Dwell Time (t) sec at (dwell) plunge period
W1	200	157	17	498	11.05	6
W2	200	127	17	471	11.43	8
W3	120	116	21	598	11.56	7
W4	120	126	20	549	11.47	6
W5	120	115	17	532	11.47	7
W6	120	105	18	583	11.78	7
W7	120	119	20	548	11.59	7

Table 3 shows the peak temperatures measured by the thermocouples for each of the welding trials. It is worth noting that in Table 3 some of thermocouple readings are missing because it either has been displaced by the FSW flash or another data recording error occurred during testing.

Table 3: Thermocouples measurements of the seven plunge trials

Weld No.	Maximum recorded Temp. T °C TC 1	Maximum recorded Temp. T °C TC 2	Maximum recorded Temp. T °C TC3	Maximum recorded Temp. T °C TC 4	Maximum recorded Temp. T °C TC 5	Maximum recorded Temp. T °C TC 6
W1	430	630	430	422	600	421
W2	444	650	-----	427	620	432
W3	380	550	381	382	545	---
W4	400	580	-----	402	581	405
W5	----	544	375	380	553	381
W6	----	----	420	410	----	----
W7	400	554	----	----	----	----

Macrographs of cross sections normal to the thermocouple locations of W1 through W7 are shown in Figure 3. The samples were polished, etched and examined using IFM. Regions affected by the welding process for all welds under study can be divided into five regions as follows: region 1 included TMAZ under the tool shoulder; region 2 was TMAZ around the probe side; region 3 for Inner HAZ (IHAZ), region 4 was Outer HAZ (OHAZ) (and finally region 5 included probe end. These regions are shown in Figure 4.
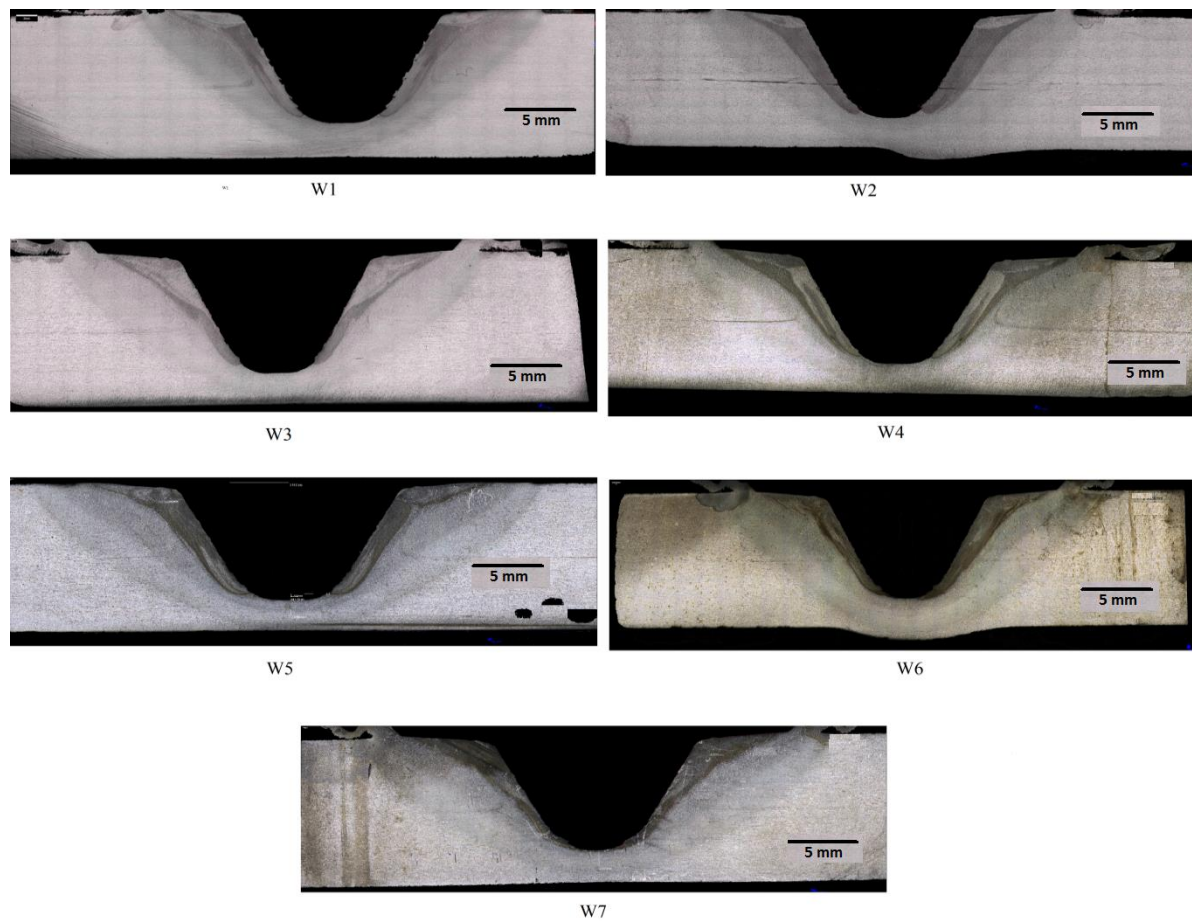

Fig. 3: Micrographs of longitudinal cross section taken from samples W1-W7, polished and etched by 2%Nital.
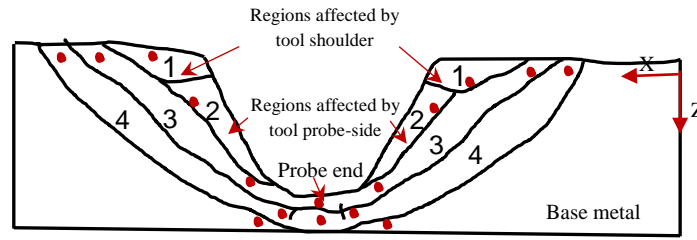
Fig. 4: Affected regions identified following weld tool plunge trials (TMAZ under shoulder (region 1), TMAZ around the probe side (region 2), Inner Heat Affected Zone IHAZ (region 3), Outer Heat Affected Zone OHAZ (region 4) and probe end). The red points refer to the location of SEM images taken for each region (figure 7a to 7h to figure 11a to 11h).

3.2 Microstructural Investigation (SEM): The as-received parent metal microstructure is shown in Fig. 5. It consists of ferrite grains (size of 20 μm on average) with bands of pearlite. Following the plunge trials, SEM micrographs showed that the microstructure of EH46 steel grade has experienced phase changes which will now be discussed for each affected regions. The locations of regions affected by tool plunge and rotation are shown in Figure 4; the red points refer to the location of SEM images as shown in Figure 7 to Figure 11.

Given that the W3, W4 and W5 have the same rotational speeds and also have very similar (and very close) plunge depth they will be considered together and their microstructures will be compared. Other welds including W1, W2, W6 and W7 will be considered separately.
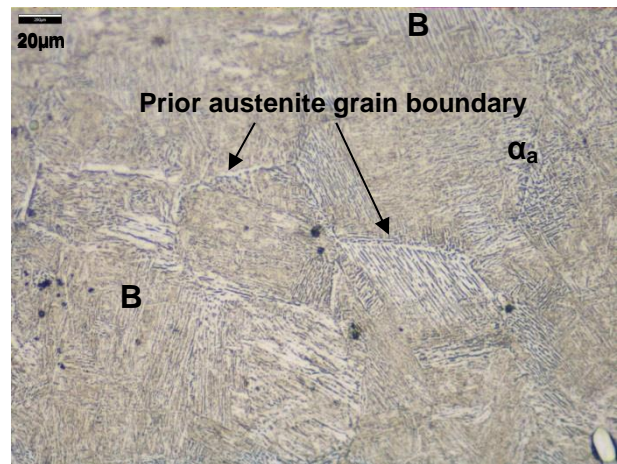

-a-   -b-
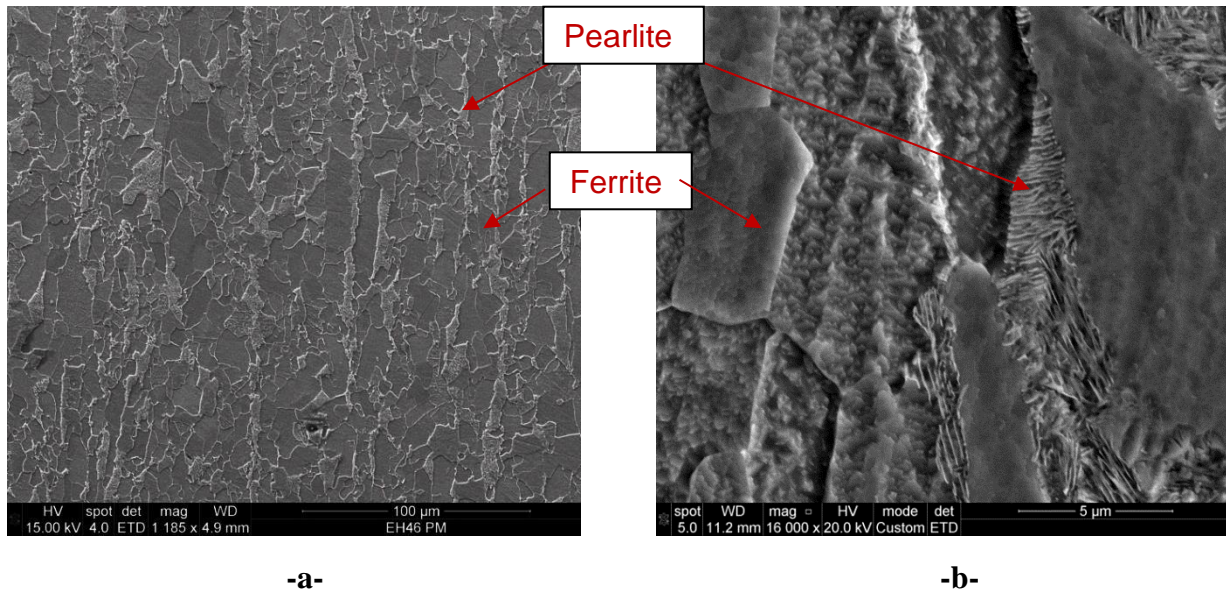
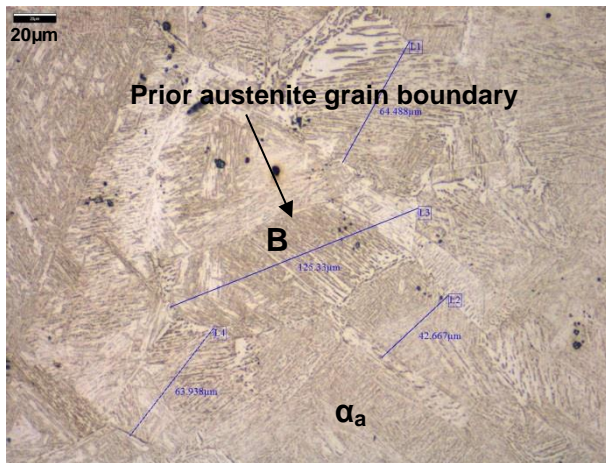**Fig. 5: EH46 as-received shows a-20 μm ferrite grains and bands of pearlite, a-Low magnification. B-High magnification.**
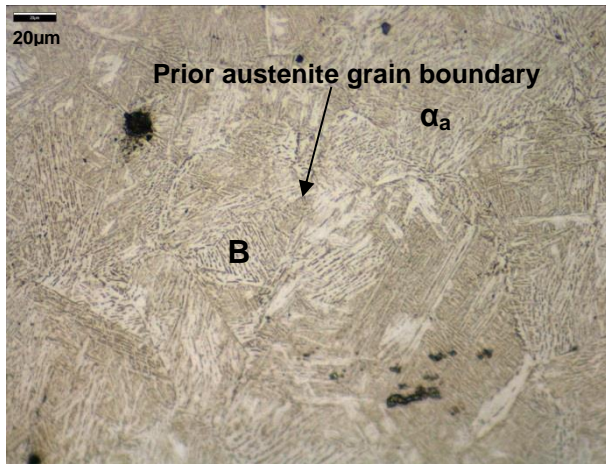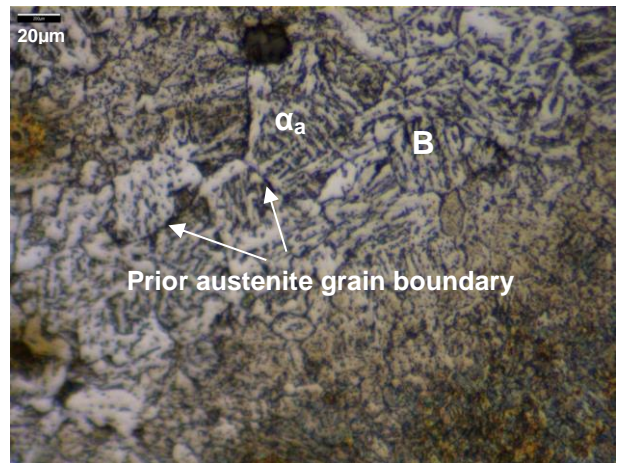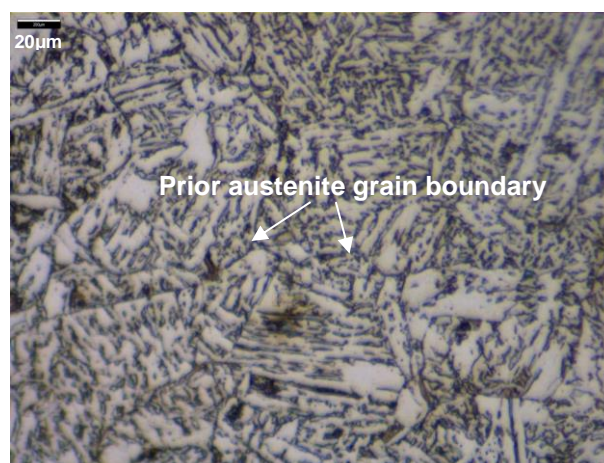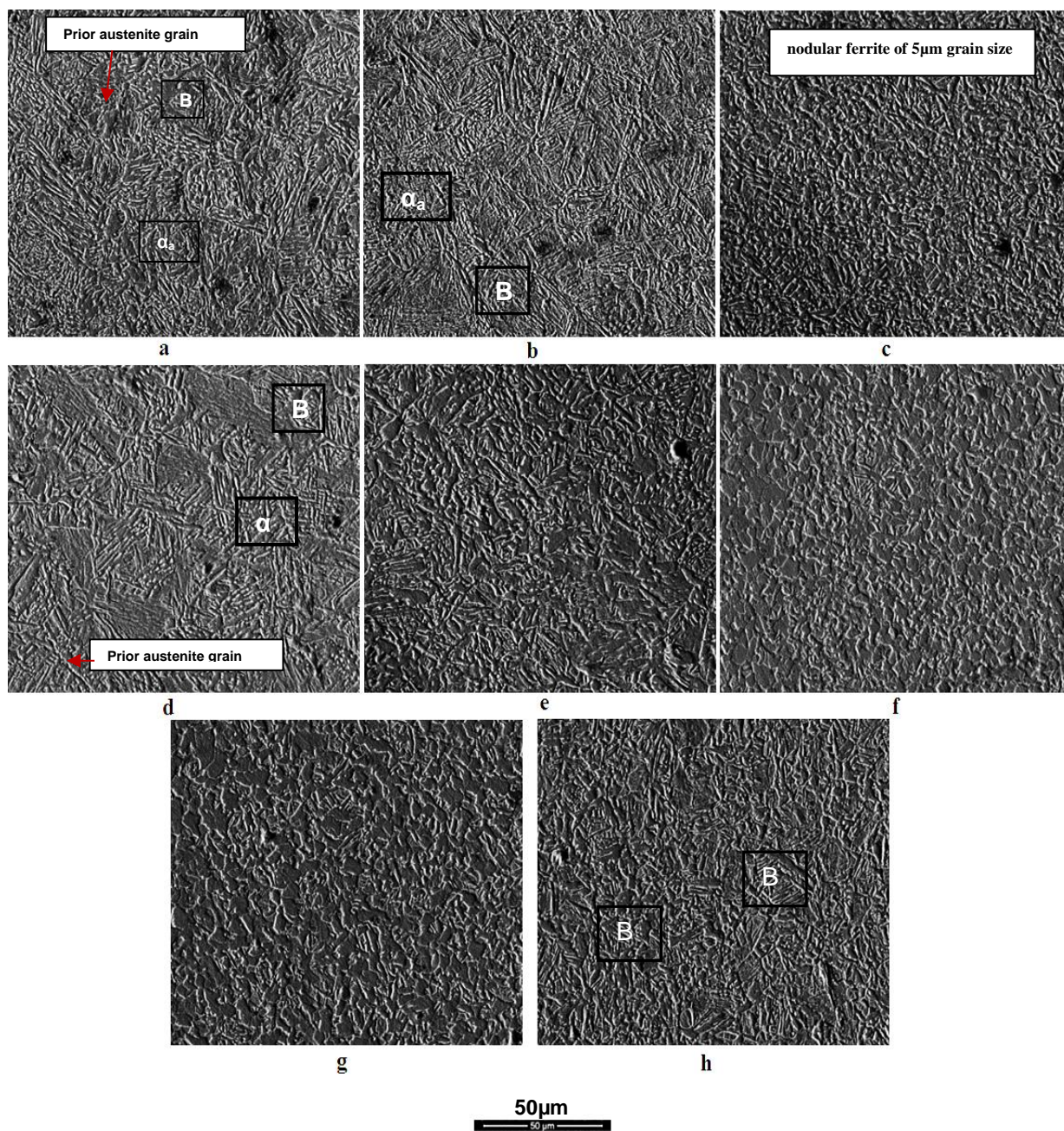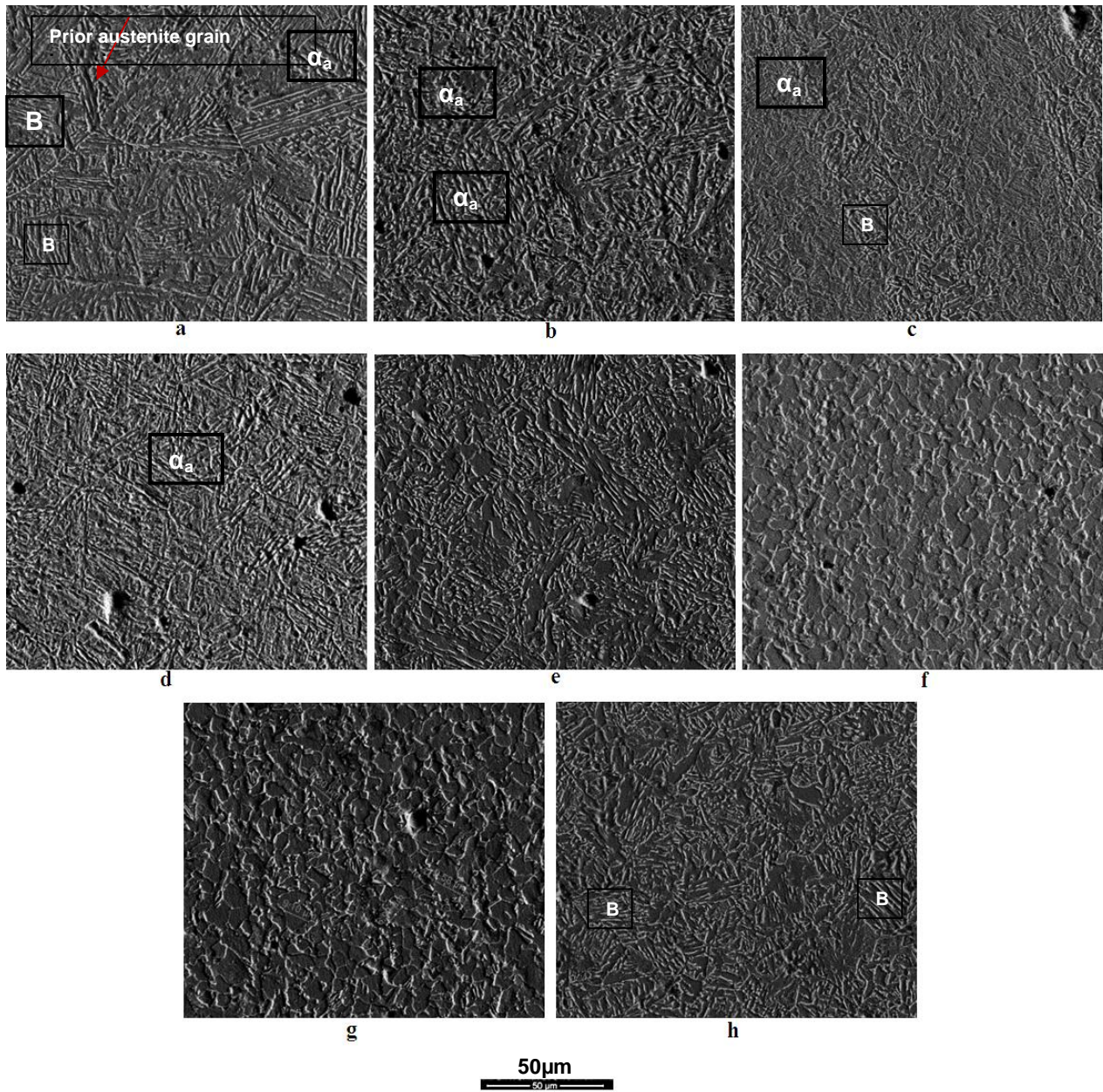
-a- W1

-b- W2

-c- W5

-d- W6

-e- W7

**Fig. 6: Optical images of region 1 for W1, W2, W5, W6 and W7.**

Fig. 7: SEM micrographs of W1 for all regions of interest: a- W1 (Region 1) under shoulder. b- W1 (Region 2) Probe side top region. c- W1 (Region 2) probe side bottom. d- W1 (Region 3) IHAZ top. -e- W1 (Region 3) IHAZ bottom, f- W1 (Region 4). g-Region 4 OHAZ bottom. h-probe end.

Fig. 8: SEM micrographs of W2 for all regions of interest. a-W2 (Region 1) under shoulder . b-W2 (Region 2) probe side top . c-W2 (Region 2) probe side bottom. d-W2 (Region 3) IHAZ-top. e-W2 (Region 3) IHAZ-bottom. f-W2 (Region 4) OHAZ-top. g-W2 (Region 4) OHAZ-bottom,. h-W2 Probe end.
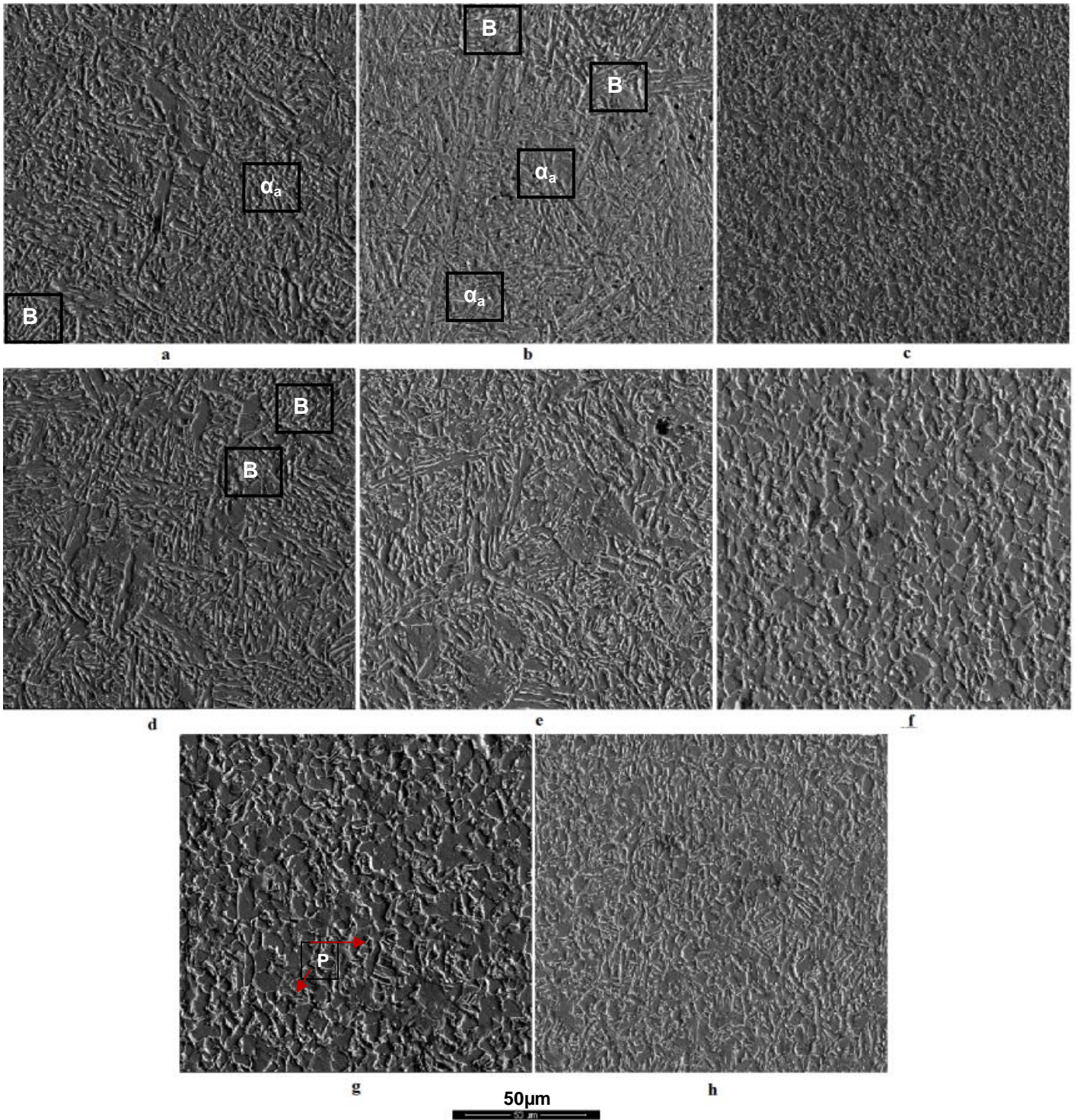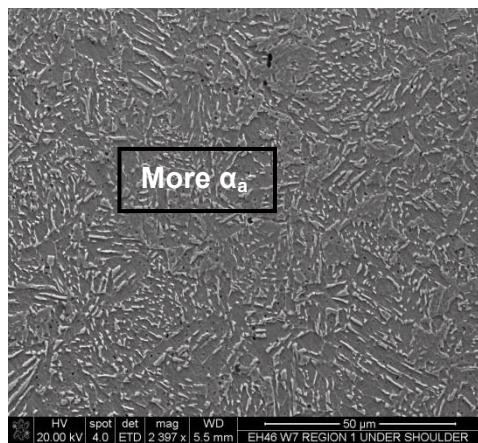
Fig. 9: SEM Micrographs of W5 for all regions of interest. a-W5 (Region 1) under shoulder. b-W5 (Region 2) probe side top. c-W5 (Region 2) probe side bottom. d-W5 (Region 3) IHAZ-top. e-W5 (Region 3) IHAZ-bottom. f-W5 (Region 4) OHAZ-top. g-W5 (Region 4) OHAZ- bottom. h-W5 Probe end.

10
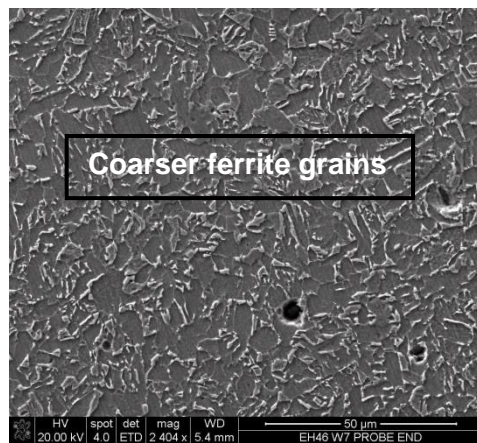
Region 1 under shoulder   **Probe end**

Figure 10: SEM Micrographs of W7, Region 1 under shoulder and Probe end.

Fig. 11: SEM micrographs of W6 for all regions of interest. a-W6 (Region 1). b- W6 (Region 2) top c-W6 Region 2-bottom. d-W6 Region 3 IHAZ top . e- W6 Region 3 IHAZ bottom, -f- W6 region 4 top. g- W6 region 4 OHAZ bottom. h-W6 probe end.

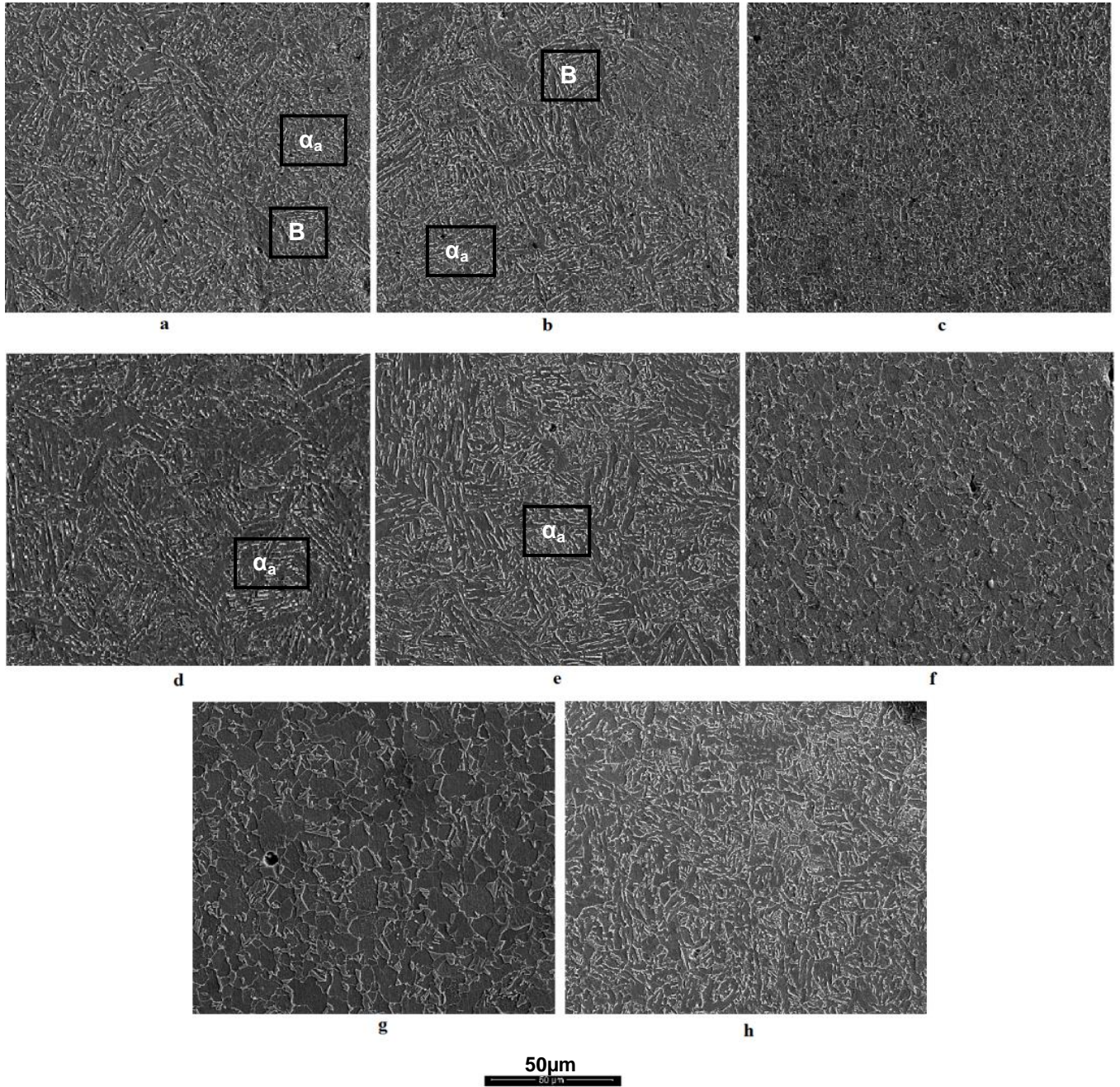Examining the results for the constant rotational speed of 200RPM (W1 and W2) it would appear that the higher plunge depth is associated with a higher average heat in-put.

W1 region1 (TMAZ under shoulder) (Fig. 6 -a-) shows a Bainite (B) phase inside prior austenite grains which has an average of 55μm grain size, as well as, some acicular ferrite phase ($α_a$). W2 region 1 (Fig. 6 -b-) shows a Bainite (B) phase with an average of 80μm prior austenite grains and some acicular ferrite phase $α_a$. The difference in prior austenite grain size between W1 and W2 asserts the reading from the thermocouple (Table 3) which showed a higher temperature at W2 probably due to the higher plunge depth and longer dwell time (Table 2). For both W1 and W2 the cooling rate at region 1 was high enough to form B phase; limited $α_a$ phase was also found. Region 2 (probe side) top of W1 (Fig. 7 -b-) is B inside prior austenite grains of 40μm, some acicular ferrite phase $α_a$ is also found. Region 2 top of W2 (Fig. 8 -b-) shows mainly acicular ferrite phase $α_a$ with limited B phase, so the peak temperature is expected to be higher and cooling rate to be slower than in W1. The finding from W1 and W2 welded samples suggests that controlling the plunge depth is more important to generate heat in FSW under a constant rotational speed and thus W2 has the higher plunge depth and has a higher percentage of acicular ferrite. Increasing plunge depth even parts of millimetre inside the workpiece can make a significant difference in heat generation and microstructure evolution. This finding is in accord with Nagasaka and Nishihara [7] who showed that increasing the plunge depth caused an increase in workpiece temperature. Fehrenbacher, et al. [8] reported that increasing plunge depth in FSW of aluminium from 4.6mm to 5mm has caused peak temperature to increase from $400^{o}C$ to 580 ^{o}C.

Region 2 bottom of W1 (Fig. 7 -c-) shows a ferrite-cementite aggregate (FCA) with nodular ferrite of 5 μm grain size. Region 2 bottom of W2 (Fig. 8 -c-) shows a mix of B with prior austenite of 20 μm grain size and some acicular ferrite phase $α_a$. As discussed previously, the effects of plunge depth (and dwell time) was apparent in generating more heat towards the sample depth in W2 compare to W1. Region 3 IHAZ top of W1 (Fig. 7 -d-) showed a mix of B with prior austenite grains of 20μm and also some acicular ferrite phase $α_a$. Region 3 IHAZ top of W2 (Fig. 8 -d-) showed mainly acicular ferrite phase $α_a$. These microstructures of both W1 and W2 indicate that temperature at the IHAZ top (Region 3 top) is still high and above the A_1 line in the Fe-C phase diagram which is enough for phase transformation of this type of steel. The bottom of region 3 showed a coarse (FCA) for W1 and a matrix of ferrite with short plated cementite in W2 (as shown in Fig. 7 -e- and Fig. 8 -e- respectively). Again from the microstructure evolution the expected temperature of W1 at this location is less than expected in W2 due to the difference in plunge depth and/or dwell time. Fig. 7 -f- and -g- show the microstructure of W1 region 4 (OHAZ) top and bottom respectively. They show nodular ferrite with 6 μm grain size in the top of region 4 while the grain size of ferrite was 7-8 μm at the bottom of this zone. Region 4 of W2 shown in Fig. 8 -f- also contained a nodular ferrite microstructure but with grain size of 10 μm, also cementite was precipitated on the grain boundaries of ferrite. The bottom of the former region as shown in Fig.8 -g- is a 9 μm ferrite grains decorated by cementite. The region just under the probe end of W1 and W2 as shown in Fig. 7 -h- and Fig. 8 -h- respectively showed a similarity in microstructure which was ferrite-cementite aggregate (FCA) and some islands of bainite with 15 μm prior

austenite grains. This similarity in microstructure in W1 and W2 at the probe end is indicative of close/similar amount of heat generation and thus similar temperatures range experienced by the material in contact with that part of the tool. This finding indicates that although the W1 microstructure experienced slightly lower temperature at the shoulder and around the probe side compared to W2, the probe end for both cases (W1 and W2) shows no evidence of a significant heat difference. Schmedit et al. 2005 [9] showed analytically that the probe end contribution in heat generation for the hybrid PCBN FSW tool was less than 3% because of a smaller probe end/workpiece contact area compared to other tool parts.

Table 4: Microstructure of the different affected regions of W3, W4, W5 and W7.

Region No.	Affected Region	Main microstructure	Average prior Austenite grains size (µm) of B phase	Estimated range of temperature (^{o}C) (Using Di Martino et al assumption)[10]	Estimated cooling rate ^{o}C/s (using Di Martino et al assumption)[10]
1	under the shoulder	Mix of bainite and acicular ferrite More acicular ferrite in W7	W03(33±2) W04(35±2) W05(40±3) W07(35±2)	1200-1300°C in the top surface and 1100-1000°C for the bainite phase	20-30 for FCA and 30-40 For B phase
2	probe side	Top of the probe side is a mix of bainite and acicular ferrite, bottom of the probe side is a fine ferrite (4-5 µm) decorated by cementite.	W03(18±1) W04(19±2) W05(20±2) W07(25±2)	1200-1300°C	30-40
3	IHAZ (Top) IHAZ (bottom)	Bainite with a coarser ferrite (2.5 µm) and cementite (1 µm) bands, the cementite bands are shorter than in regions 1 and 2 Longitudinal ferrite matrix with a mix of longitudinal and nodular cementite	15±2	1100-1000°C	20-25
4	OHAZ	Ferrite matrix with cementite precipitated on the grain boundaries, [nodular ferrite grain measured 7-8 µm] the microstructure in welds tends to be ferrite grains (9 µm) decorated by cementite with some islands of pearlite toward the bottom of this region	not clear	1000-900 ^{o}C	25-30
----	probe end	Ferritic matrix with fine (0.3 µm) short plate-like cementite Coarser grains in W7	not clear	1000-1100 ^{o}C	20-30 for FCA and 30-40 For B

W3, W4, W5 and W7 showed some similarity in microstructure and thus their description was organised in Table 4. Fig. 8 shows the macrograph of W5 and the microstructure of regions of interest. A comparison in microstructure of these welds with W1 and W2 are carried out here. The microstructure at region 1 of W1 and W2 (Fig. 6 -a- and -b-) which showed a B phase with prior austenite grains larger than of the 120 RPM group as shown in Table 4 shows that the peak temperatures at the shoulder/workpiece contact region was higher in W1 and W2. This finding is in accordance with other work [9], [11] and [12] which indicates that heat input increases with the tool rotational speed. Region 2 top and bottom of W2 showed also a microstructure evolution with an expected temperature (readings of TC2 and TC5 in Table 3) higher than 120 RPM group because of the higher rotational speed. This indicates that in W2 the rotational speed effect was overriding the slight increase in plunge depth of 120RPM group. W1 showed some similarity in microstructure of 120RPM group in Table 4 at region 2 top and bottom, however, the prior austenite grains of W1 at region 2 top was double. This similarity in microstructure despite the higher rotational speed of W1 than group of 120RPM (shown in Table 4) can be related to the difference (about 0.5mm Table 2) in the plunge depths. The increase in plunge depth (exceed 11mm) in 120RPM group has caused an increase in the contact area between tool and workpiece and thus produces more heat towards the plate thickness. W7 microstructure under the tool shoulder shows more acicular ferrite compare to W3, W4 and W5 while the probe end showed coarser ferrite grains as shown in figure 4.99 which indicate that more heat input is produced during FSW process as a result of increasing the plunge depth to about 0.1mm.

Fig. 11 shows the microstructure of W6 for all regions of interest. Although the rotational speed of W6 was the same of W3,W4,W5 and W07, it shows some difference in microstructure evolution especially in the direction towards the probe end. A mix of acicular ferrite microstructure and B phase with prior austenite grains of (35 µm) was found under shoulder in region 1 as shown in Fig. 6 -d-. This microstructure is similar to the one found in other group of 120RPM. This finding support the assertion that increasing plunge depth is highly affected on the microstructure towards the sample depth but less on the top. Region 2 top (Fig. 11 -b-) showed higher amount of acicular ferrite microstructure similar to that found in W2. Compare to other cases of 120RPM shown in Table 4 which showed a mix of B and acicular ferrite, region 2 top of W6 seem to be experienced higher temperature and slower cooling rate and thus the microstructure of acicular ferrite was dominated. Region 2 bottom (Fig. 11 -c-) showed ferrite grains (7 µm) with cementite precipitate at the grain boundaries. Region 3 (IHAZ) showed acicular ferrite in the top and a mix of acicular ferrite and nodular ferrite in the bottom. This microstructure evolution is certainly experienced higher temperature compare to the microstructure of other 120RPM group which shows a mix of B and FCA because of the difference in plunge depth as shown in Table 1. The microstructure of W6 region 3 is also similar to that found in W2, however, W6 region 3 bottom showed some nodular ferrite in addition to short plated cementite. Region 4 OHAZ showed ferritic grains of (7-8 µm) with a mix of short plated and nodular cementite. Probe ends showed a ferritic matrix with short plated cementite (FCA) microstructure which was almost similar to other 120RPM welds. It was also similar to 200RPM group, however, some B phase was found in W1 and W2. From all studied cases it can be inferred that the microstructure

evolution was spatial. Regions in contact with and near the tool have showed a higher phase transformation rather than other regions because of receiving higher heat input. It is also shown from the macrographs in Figure 3 that the regions affected by the tool probe is bigger (represent about 70% from the total TMAZ and HAZ) than those affected by the tool shoulder, thus it can be suggested that FSW tool with a stationary shoulder and slightly higher rotational speed can be enough for generating the heat required for welding.

Given that all studied cases have experienced phase transformations in the TMAZ region (regions 1 and 2 combined together); hence this area should have fully been austenitised during the plunge/dwell. This region, which is also called the shear layer [10], is believed to experience material flow when its temperature rises above the A3 line of Fe-C phase diagram.

Conclusion

-Heat input increase with increasing the rotational speed of the FSW tool, from 120 RPM to 200 RPM, especially in the tool shoulder/workpiece contact surface.

-Increasing plunge depth is significantly affected on the microstructure towards the sample depth; a tenth of a millimetre can vary the microstructure from one sample to another. For example in W6 under the shoulder region, in a mixture of bainite and ferrite, more acicular ferrite was observed when the plunge depth was increased. Increasing the plunge depth produced more heat input than increasing the tool rotational speed. This was attributed to the fact that more tool surface area was in contact with the workpiece when plunge depth was increased.

-The Probe side played a significant role in stirring material and heat generated around it.. In contrast probe end did not show a significant effect in stirring the material. Based on the results it is suggested that a tool with stationary shoulder and rotating probe would be sufficient to complete the welding process at a reduced cost.

-In all studies plunge/dwell experiments it was found that microstructure of flow regions 1 and 2 (total TMAZ) was fully austenite. This suggests that steel flow mostly occurs above the A_3 line in the Fe-C phase diagram.

Acknowledgement

References

1. A.Toumpis, A. Gallawi, S. Cater, L. Molter:, A techno-economic evolution of friction stir welding of DH36 steel, 10th Friction Stir Welding Symposium ,10th FSWS, 20-22/05/2014, Beijing pp.1-11. (2014).

*2. Z. Feng, M. L. Santella, S. A. David, R.J. Steel, S. M. Packer, T Pan, M. Kuo and R. S. Bhatnagar, Friction Stir Spot Welding of Advanced High-Strength Steels –A Feasibility Study, SAE technical paper, Vol., No.
2005-01, pp. 1248, (2005).*

3. Lomholt, C. Trine ; Pantleon, Karen ; Somers, A.J. Marcel ; Adachi, Yoshitaka ; Peterson, Jeremy ;Steel, Russell: Microstructure Characterization of Friction Stir Spot Welded TRIP Steel, Advanced Materials Research, Vol.409, pp.275-280., (2012).

4. C. C. P. Mazzaferro, T. S. Rosendo, M. A. D. Tier, J. A. E. Mazzaferro, J. F. Dos Santos and T. R. Strohaecker, Microstructural and Mechanical Observations of Galvanized TRIP Steel after Friction Stir Spot Welding, Materials and Manufacturing Processes, 30: 1090–1103, (2015).

5. Y. Hovanski, M.L. Santella, G.J. Grant. FSSW in Hot-Stamped Boron Steel, Scripta Materialia 57 873-876. (2007).

6. M.Miles, T.Hartman, C. Cunningham, N. Saunders ; Y. Hovanski: High Speed Friction Stir Spot Welding of Advanced High Strength Steel, Material Science and Technology Conference and Exhibition, 7-11 October Pennsylvania, USA, Volume 1 of 2.(2012).

7. Nagasaka and Nishihara: Measurement of tool temperature during friction stir welding, Proceeding of forth international symposium on FSW, Park city, Utah. (2003).

8. Fehrenbacher , A., Schmale, J. R., Zinn, M. R., & Pfefferkorn, F. E. (2014). Measurement of Tool-Workpiece Interface Temperature Distribution in Friction Stir Welding. Journal of Manufacturing Science and Engineering, 136(2), 21009

9. H. Schmidt and J. Hattel: Modelling heat flow around tool probe in friction stir welding. Science and Technology of Welding and Joining, 10(2), pp.176–186. (2005).

10. Di Martino ,Thewlis S.F, 2013. Transformation Characteristics of Ferrite/Carbide Aggregate in Continuously Cooled, Low Carbon-Manganese Steels. Metallurgical and Materials Transactions A, 45(2), pp.579–594.

11.S. Rajiv Mishra; W. Murray, Mahoney: Friction Stir Welding and Processing, (ASM International. 2007), pp 163-167.

12. M. Al-moussawi, A. Smith, A. Young, S. Cater and M. Faraji,2016, An advanced numerical model of friction stir welding of DH36 steel, 11th Int. Symp. FSW, TWI Granta Park Cambridge, UK.